DMD Fast Forward. Published on October 9, 2014 as DOI: 10.1124/dmd.114.059378
This article has not been copyedited and formatted. The final version may differ from this version.

Enhanced methamphetamine metabolism in rhesus macaque as compared to human: An analysis using a novel LCMS/MS method, kinetic study, and substrate docking

Ravinder Earla, Santosh Kumar, Lei Wang, Steven Bosinger, Junhao Li, Ankit Shah, Mohitkumar Gangwani, Anantha Nookala, Xun Liu, Lu Cao, Austin Jackson, Peter S. Silverstein, Howard S. Fox, Weihua Li, Anil Kumar

Division of Pharmacology and Toxicology, School of Pharmacy, University of Missouri-Kansas City, Kansas City, Missouri, 64108 (R.E., A.S., M.K.G., A.N., X.L., L.C., A.J., P.S.S., A.K.)

Department of Pharmaceutical Sciences, College of Pharmacy, University of Tennessee Health Sciences, Memphis, Tennessee 38163(S.K.)

Shanghai Key Laboratory of New Drug Design, School of Pharmacy, East China University of Science and Technology, Shanghai 200237, China (L.W., J.L., W.L.)

Yerkes National Primate Research Center of Emory University, Atlanta, Georgia 30322 (SB); University of Nebraska Medical Center, Omaha, Nebraska 68198 (H.S.F.)

DMD Fast Forward. Published on October 9, 2014 as DOI: 10.1124/dmd.114.059378
This article has not been copyedited and formatted. The final version may differ from this version.

Running title: CYP-mediated methamphetamine metabolism in rhesus and human

Corresponding authors

Ravinder Earla, Ph.D. School of Pharmacy, University of Missouri-Kansas City, 2464 Charlotte Street, Kansas City, Missouri 64108, Tel: 816-235-1793, Fax: 816-235-1776, Email: earlar@umkc.edu;

Santosh Kumar, Ph.D., Department of Pharmaceutical Sciences, College of Pharmacy, University of Tennessee Health Sciences, 881 Madison Ave., Memphis, TN 38163, Tel: 901-448-7157, Email: ksantosh@uthsc.edu;

Number of pages: 39

Number of tables: 6

Number of figures: 6

Number of references: 53

Total words in the abstract: 248

Total words in the introduction: 805

Total words in the discussion: 1508

ABBREVIATIONS: CV, Coefficient of variation; CYP, Cytochrome P450; MA, Methamphetamine (*d & l*); 4-OH MA, 4-hydroxymethamphetamine; AM, Amphetamine; 4-OH AM, 4-hydroxyamphetamine; ESI, Electrospray ionization; GC-MS, Gas chromatography mass spectrometry; HPLC, High performance liquid chromatography; IS, Internal standard; LC-MS/MS, liquid chromatography tandem mass spectrometry; LLOQ, Lower limit of quantitation; MRM, Multiple reactions monitoring; *m/z*, Mass-to-charge ratio; QC, Quality control; ULOQ, Upper limit of quantitation; SPE, Solid phase extraction; NHP, Nonhuman primate.

DMD Fast Forward. Published on October 9, 2014 as DOI: 10.1124/dmd.114.059378
This article has not been copyedited and formatted. The final version may differ from this version.

ABSTRACT

Methamphetamine (MA), which remains one of the widely used drugs of abuse, is metabolized by the cytochrome P450 (CYP) family of enzymes in humans. However, metabolism of methamphetamine in macaques is poorly understood. Therefore, we first developed and validated a very sensitive LC-MS/MS method using solid phase extraction of rhesus plasma with a lower limit of quantitation at 1.09 ng/mL for MA and its metabolites, 4-hydroxy methamphetamine (4-OHMA), amphetamine (AM), 4-OH amphetamine (4-OHAM), and norephedrine. We then analyzed plasma samples of MA-treated rhesus, which showed >10-fold higher concentrations of AM (~29 ng/mL) and 4-OHAM (~28 ng/mL) than MA (~2 ng/mL). Since the plasma levels of MA metabolites in rhesus were much higher than in human samples, we examined MA metabolism in human and rhesus microsomes. Interestingly, the results showed that AM and 4-OHAM were formed more rapidly and the catalytic efficiency (V_{max}/K_m) for the formation of AM was ~8-fold higher in rhesus than in human microsomes. We further examined the differences in these kinetic characteristics using three selective inhibitors of each human CYP2D6 and CYP3A4 enzymes. The results showed that each of these inhibitors inhibited both *d*- and *l*-MA metabolism by 20-60% in human microsomes, but not in rhesus microsomes. The differences between human and rhesus CYP2D6 and CYP3A4 enzymes were further assessed by docking studies for both *d*- and *l*-MA. In conclusion, our results demonstrated an enhanced MA metabolism in rhesus compared to human, which is likely to be caused by differences in MA-metabolizing CYP-enzymes between these species.

DMD Fast Forward. Published on October 9, 2014 as DOI: 10.1124/dmd.114.059378
This article has not been copyedited and formatted. The final version may differ from this version.

INTRODUCTION

Methamphetamine (MA) remains one of the widely used drugs of abuse. MA abuse can cause euphoria, dysphoria, paranoia, cognitive impairments and neuronal toxicity. It also decreases the dopamine and serotonin levels in the brain (Thompson et al., 2004; Krasnova and Cadet, 2009). Similar findings were also observed in other species including monkey, rat, and mouse brain (Melega et al., 2008; Krasnova and Cadet, 2009). Although, the altered level of dopamine can result in MA-mediated neurotoxicity and an increase in oxidative stress, (Fitzmaurice et al., 2006) the underlying mechanisms remain unclear. Cytochrome P450 (CYP)-mediated metabolism of various drugs, including MA, can lead to oxidative stress, which may cause neurotoxicity (Lin et al., 1997; Cherner et al., 2010; Moszczynska and Yamamoto, 2011; Pendyala et al., 2011; de la Torre et al., 2012; Shah et al., 2013); (Dorman et al., 2008). While many pathological conditions that afflict humans can be accurately recapitulated in mouse models, nonhuman primate (NHP) models still play the preeminent role in research concerning many diseases. This is especially so in the area of infectious disease research concerning pathogens such as HIV-1 and tuberculosis (Legrand et al., 2009; Holder et al., 2014; Phillips et al., 2014; Scanga and Flynn, 2014), as the host-pathogen interactions involved in these pathologies are most accurately reproduced in a NHP model. In these diseases, as well as others, NHP models are often used to test the efficacy of therapeutic agents that are metabolized by the CYP450 pathway (Nishimuta et al., 2011; Uno et al., 2014). Even though the NHP models can accurately reproduce the pathogenic effects of the pathogen as well as model drug disposition, the use of drugs of abuse must also be taken into account. Not only do these agents have the potential to alter the pathological course of disease by affecting the inflammatory process, they also have the ability to modify the effects of therapeutic agents by affecting their metabolism and/or disposition (Nishimuta et al., 2010; Moss et al., 2012; Uno et al., 2014). However, MA metabolism in macaques is poorly

understood. Therefore, given the wide use of rhesus macaques concerning infectious diseases that have a high prevalence among users of MA, here we investigated CYP-mediated MA metabolism in rhesus macaques.

MA is primarily metabolized to amphetamine (AM) and 4-hydroxy methamphetamine (4-OH MA) (de la Torre et al., 2012) by human CYP2D6 and, to a lesser extent, by CYP3A4 (Welter et al., 2013). AM is further metabolized to 4-hydroxymethamphetamine (4-OH AM) and norephedrine by CYP2D6 (Miranda et al., 2007; de la Torre et al., 2012). Many species of monkeys, including rhesus macaques, also express various CYP-isozymes that are homologous to human CYP2D6 and CYP3A4 with >90% homology (Carr et al., 2006; Uno et al., 2010). These enzymes in monkeys may also be responsible for the metabolism of MA, but that connection is unknown. Therefore, we studied MA metabolism in rhesus macaques, and compared the results with MA metabolism in human. However, in order to study MA metabolism in rhesus, we first need to develop a sensitive liquid chromatography tandem mass spectrometry (LC-MS/MS) method to measure MA and its metabolites in rhesus plasma and liver microsomes.

In previous studies, MA and its metabolites have been quantified in brain, urine, serum, plasma, hair, and nails using immunoassay, HPLC, GC-MS, and LC-MS (Fitzgerald et al., 1988; Thurman et al., 1992; Armstrong and Noguchi, 2004; Berankova et al., 2005; Hendrickson et al., 2006; Kim et al., 2008; Wongniramaikul et al., 2012; Koster et al., 2014). However, these methods have moderate sensitivity with a lower limit of quantitation (LOQ) at 5-10 ng/mL. In addition, these methods can be laborious and time consuming (Armstrong and Noguchi, 2004; Kim et al., 2008). Recently, additional LC-MS/MS methods have been developed to study MA metabolism in human; however, these methods are less sensitive, time consuming and tedious (Djozan and Baheri, 2007; Sergi et al., 2009; Lee et al., 2012). To study extensive MA metabolism, a suitable and sensitive analytical method is needed for

the determination of MA and its four MA metabolites such as 4-OH MA, AM, 4-OH AM, and norephedrine. These four metabolites are important since they are the most active sympathomimetic agents compared to other MA metabolites (Kraemer and Maurer, 2002). As such there is no appropriate validated LC-MS/MS method reported for the determination of MA and its metabolites in rhesus plasma and liver microsomes. Therefore, we developed and validated a novel, sensitive, and rapid ESI LC-MS/MS method using solid phase extraction (SPE) from plasma and liver microsomes of human and rhesus monkey for concurrent analysis of MA and four of the metabolites. We then studied the relative metabolism of MA stereoisomers (*d*- and *l*-MA) in rhesus and human liver microsomes using enzyme kinetics and inhibition methods. Further, we performed a docking study to explain the results obtained from the kinetic and inhibition studies.

DMD Fast Forward. Published on October 9, 2014 as DOI: 10.1124/dmd.114.059378
This article has not been copyedited and formatted. The final version may differ from this version.

MATERIALS AND METHODS

Chemical and Reagents: MA, 4-OH MA, AM, 4-OH AM, norephedrine, MA-d5, and AM-d8, and CYP inhibitors were purchased from Cerilliant Analytical Reference Standards (Sigma-Aldrich Company, Round Rock , TX). HPLC grade methanol, acetonitrile, ammonia, and formic acid were purchased from Fisher Scientific (New Brunswick, NJ). All HPLC grade chemicals were utilized without further purification. An Xbridge HPLC reverse phase C18 column and HLB Oasis solid phase extraction cartridges (Waters Corporation, Milford, MA) were employed for the determination of analytes.

Method development: MA, 4-OH MA, AM, 4-OH AM, norephedrine, MA-d5, and AM-d8 stocks were made in methanol and concentrations were corrected using the formula described earlier (Earla et al., 2012). Standard curves (800.00, 640.00, 486.40, 389.12, 214.02, 74.91, 14.98, 4.94, 1.09 ng/mL) for each analyte were generated using drug-free rhesus macaque plasma. Similarly, the quality control (QC) samples at four concentrations (486.40, 214.02, 14.98 and 1.09 ng/mL) were separately prepared in the rhesus plasma as mentioned earlier (Earla et al., 2012). The system suitability test for each analyte was performed independently by using six replicate injections of 800 ng/mL of the reference standard with internal standard (IS). The carry-over test was performed by injecting an extract blank followed by immediate injection of an extracted upper limit of quantitation (ULOQ) of the standard curve with an IS. The liquid chromatography tandem mass spectrometry (LC-MS/MS) method was developed using rhesus plasma. The mass spectrometer (3200 QTRAP LC-MS/MS system, AB Sciex) was optimized for detection of MA and its four metabolites along with IS. The most suitable proton adduct in an electrospray ionization $[M+H]^+$ precursor ions was determined for MA (150.5), 4-OH MA (166.3), AM (136.4), 4-OH AM (152.3), norephedrine (152.3), MA-d5 (155.5), and AM-d8 (144.5) (Fig. 1 and Supplemental Table 1). These precursor ions were optimized by adjusting the curtain gas, declustering potential, ion spray voltage, and source

DMD Fast Forward. Published on October 9, 2014 as DOI: 10.1124/dmd.114.059378
This article has not been copyedited and formatted. The final version may differ from this version.

gas 1. The precursor ions of MA and four of its metabolites along with IS were fragmented by applying collisionally-activated dissociation gas and collision energy to obtain their most abundant product ions. The product ions for MA (91.2), 4-OH MA (135.4), AM (91.3), 4-OH AM (135.2), norephedrine (134.4), MA-d5 (92.3), and AM-d8 (97.2) were optimized as described in our earlier report (Earla et al., 2014) (Fig.1 and supplemental Table 1). The multiple reactions monitoring (MRM) transitions (*m/z*) $[M+H]^+$, (Q_1/Q_3) selected for quantitative analyses were: 150.5/91.2 for MA, 166.3/135.4 for 4-OH MA, 136.4/91.3 for AM, 152.3/135.2 for 4-OH AM, 152.3/134.4 for norephedrine, 155.5/92.3 for MA-d5, and 144.5/97.2 for AM-d8 (Fig. 2 and Supplemental Table 1). A dwell time of 200 ms and a source temperature of 450°C was employed for all the analyte determinations.

The chromatographic separation was achieved using a reverse phase Xbridge MS C18 column (50x4.6 mm, i.d, 5µm) in conjunction with a UFLC Shimadzu LC-20AD HPLC (California, USA). An isocratic mobile phase composed of 65% acetonitrile and 35% of water containing 0.05% of formic acid at a flow rate of 0.3 mL/min was used. The samples were reconstituted in 200 µL of mobile phase and 10 µL of each sample was injected into the LC-MS/MS for quantitative analysis over a 4 min run time. The LC-MS/MS acquired MRM data was processed using Analyst software (version 6.2). A simple SPE technique was used for extraction of analytes. Macaque plasma was spiked with 20 µl of 10 µg/ml IS (final concentration of ~1 µg/ml). The mixture was vortex-mixed for 30 sec followed by the addition of 20 µL of an aqueous 10% formic acid solution, which was again vortex-mixed for one min prior to SPE. The SPE columns (HLB 30 mg, 1 mL cartridge) were conditioned with 1 mL of methanol followed by 1mL of water. After loading, washing and drying of the SPE

DMD Fast Forward. Published on October 9, 2014 as DOI: 10.1124/dmd.114.059378
This article has not been copyedited and formatted. The final version may differ from this version.

cartridge as described previously (Earla et al., 2014), analytes were eluted with 1 mL methanol. After elution, samples were evaporated using a speed vacuum at 35°C for 60 min.

Method validation: The LC-MS/MS method validation was performed by testing specificity, selectivity, accuracy, precision, recovery, matrix effect, and stability of each analyte in rhesus plasma and liver microsomes as described previously (Earla et al., 2010; Earla et al., 2012; Earla et al., 2014). The specificity and selectivity of the method were tested by analyzing blank plasma samples from six rhesus macaques for the extracted lower limit of quantitation (LLOQ, 1 ng/mL). The blank matrix signal to noise ratio did not show measurable interference at the analyte peak of interest for MA and its metabolites (Fig. 2A). The percentage of interference determined in the blank was calculated by comparing the mean peak area of LLOQ of the analyte with the peak response obtained from the blank samples (≤20%). Within-assay & between-assay, precision & accuracy experiments were performed by analyzing eight extracted calibration standards and four levels of QC standards as described earlier (Earla et al., 2010). The precision and accuracy were calculated within the acceptable range (20-25%) according to the guidance for industry bioanalytical method validation in U.S. Food and Drug Administration guidelines (www.fda.gov) and also described previously (Earla et al., 2010; Earla et al., 2014). Recovery of MA and its metabolites was estimated by analyzing two sets of six replicates of plasma extracted low and high QC standards and post-spiked (represent 100% recovery) sample along with IS. Similarly, matrix effect of MA and its metabolites was evaluated by analyzing 2 sets of six replicates of each low and high QC standards from post-spiked (extracted blank plasma samples), and spiked standards in aqueous solutions (representing no matrix effect) (Earla et al., 2014). The stability of analytes such as bench top, and freeze-thaw in rhesus plasma was studied at -80°C and 25°C, respectively for several weeks to estimate the degradation of

DMD Fast Forward. Published on October 9, 2014 as DOI: 10.1124/dmd.114.059378
This article has not been copyedited and formatted. The final version may differ from this version.

analytes in the matrix. Six replicates of each stability experiment sample at concentrations of 486.40 and 14.98 ng/mL were prepared for each analyte in pooled rhesus plasma according to our published methods (Earla et al., 2010; Earla et al., 2014).

Analysis of MA metabolism in plasma: The rhesus macaques (*Macaca mullata* of Indian origin) were bred in the Emory University breeding facility and were housed at the Yerkes National Primate Research Center as per the standards of the Association for the Assessment and Accreditation of Laboratory Animal Care. All the studies were carried out in accordance with the recommendations of the Emory University Institutional Animal Care and Use Committee under the National Institutes of Health guidelines. After the initial quarantine phase, the animals were adapted to saline injection twice every day for 4 weeks. The animals were then treated with increasing dose of MA injections (0.1 mg/kg o.i.d. - 0.75 mg/kg b.i.d.; 5 days a week) over 4-week period. The animals were then maintained at 0.75 mg/kg of MA twice every day for an additional 16 weeks to mimic conditions of chronic MA use. The blood samples were collected from the femoral vein on Monday morning after monkeys were injected with 10 doses of methamphetamine every week. The blood samples in heparin were collected after 20 weeks of methamphetamine injection. The samples were then centrifuged at 2500 rpm at 4°C for 10 min and the plasma of each sample was collected (Kumar et al., 2000; Kumar et al., 2001). All the samples were stored at -80°C until analysis and were processed according to the sample preparation and extraction protocols described in the above sections.

MA metabolism in liver microsomes: The human and rhesus liver microsomes **(**Invitrogen Corporation, Allen Way Carlsbad, CA) were used to study MA metabolism. The reaction was performed in HEPES buffer (0.1M, pH 7.4) using 1 µM MA, 1 mg/mL of microsomes (major source of CYP enzymes), 10 mM $MgCl_2$ and 1 mM NADPH at 37°C as described earlier

(Meyer et al., 2008). The reaction was initiated by the addition of NADPH and it was quenched by freezing the sample at -80°C. The reaction was performed at various time points (0, 0.5, 1, 2, 3, 6, 12 and 24 hrs). MA and its metabolites were analyzed using SPE and LC-MS/MS methods by optimizing these methods in liver microsomes (Supplemental Tables 3-5). The apparent kinetic parameters for the degradation of MA and formation of AM and 4-OH AM were determined by fitting the hyperbolic equation using Sigma plot 11. We also performed concentration-dependent kinetics using both *d*- and *l*-MA stereoisomers at various concentrations (2.5, 5, 10, 25, 50, 100, 250, and 500.0 µM) with human and rhesus microsomes. The reaction was performed as described above for 20 min at 37°C. The analysis of the formation of AM from both the MA stereoisomers by human and monkey liver microsomes were performed with Michaelis-Menten kinetics using non-linear regression (Sigma Plot software; Systat Software, Inc., San Jose, CA). For inhibition studies, the reaction mixture was pre-incubated with various inhibitors (0.5 µM of each quinidine, paroxetine, fluoxetine, ketoconazole, ritonavir, or indinavir) at 37°C for 10 min. Then, the reaction was performed as described above for 60 min. The formation of the major metabolite, AM, was measured with/and without CYP inhibitors.

MA docking to human and rhesus CYP models: The initial models of human CYP2D6 and CYP3A4 for docking were taken from Protein Data Bank (PDB). To date, there are 4 crystal structures available for human CYP2D6 and 17 for human CYP3A4. These structures were resolved with or without a ligand bound to the respective CYPs. On the basis of the resolution, completion, and ligand size, 3DTA (2.67 Å) and 3NXU (2.00 Å) were selected for human CYP2D6 and CYP3A4, respectively. Chain A of the two structures was used for docking simulations. The initial model of rhesus CYP2D6 was constructed by the comparative protein modeling method by satisfaction of spatial restraints was used to predict the 3D structural models of CYP2D6 and CYP3A64 (Larkin et al., 2007; Edmund et al.,

2013). For rhesus CYP3A64, which is homologues to human CYP3A4 (93% sequence identity) and shows similar metabolic characteristics to human CYP3A4 (Carr et al., 2006) was used to build the protein model. The 3DTA CYP2D6 and 3NXU CYP3A4 structures were chosen as the templates for the model construction of rhesus CYP2D6 and CYP3A64, respectively. Construction of the homology models was accomplished by using Modeller 9 (Fiser and Sali, 2003). The sequence alignment was performed using the default parameters by ClustalX (Larkin et al., 2007; Edmund et al., 2013). The BLOSUM matrix was used for the sequence alignments. Because of the high sequence identity between the template and the target sequence (~93% for both), there are no gap inserts for both CYP2D6 and CYP3A4 sequence alignments. Automated docking of the substrate MA into the active site of four enzymes (human CYP2D6 and CYP3A4 as well as rhesus CYP2D6 and CYP3A64) was performed using "Glide 5.8 with the standard precision mode" (http://www.schrodinger.com/citations/41/5/1/). The center of the grid was placed on the heme iron atom and the sizes of the grid box and the inner box were set to 20 Å and 14 Å, respectively. Each run has 30 outputs of the ligand poses. The first ten of binding poses with the lowest scores were analyzed in details.

Statistical analysis: The concentration of all analytes in the plasma from subjects was calculated by Analyst software (AB Sciex, Foster City, CA). The statistical significance (p-values) was calculated using one-way analysis of variance. The MA kinetic parameters were calculated using Sigma Plot software, Systat Software, Inc., San Jose, CA.

DMD Fast Forward. Published on October 9, 2014 as DOI: 10.1124/dmd.114.059378
This article has not been copyedited and formatted. The final version may differ from this version.

RESULTS

Method developments: The maximum intensity precursor ion with proton adducts $[M+H]^+$ for MA, 4-OH MA, AM, 4-OH AM, norephedrine, MA-d5, and AM-d8 was optimized by modifying the compound parameters of quadruple 1 (Q1), especially declustering potential at 30, 30, 30, 26, 30, 30 and 26 V, respectively. The collision energy of Q2 was applied to optimize the product ions of MA, 4-OH MA, AM, 4-OH AM, norephedrine, MA-d5, and AM-d8 at 15, 15, 15, 26, 12, 20 and 15 V, respectively (Table 1). The parameters for MRM transitions of Q1 and Q3 for quantitative analysis of MA and its metabolites are shown in Fig. 1 and supplemental Table 1. The system performance test resulted in <3% variation for MA and its metabolites. The %CV for MA and 4-OH MA with respect to MA-d5 as IS were 2.8 and 2.2, respectively (supplemental Table 2). Similarly, the %CV for AM, 4-OH AM, and norephedrine with respect to AM-d8 were 2.5, 2.1, and 2.7, respectively. The carry-over test for MA and its metabolites at the upper limit of quantification of the calibration curve standard did not produce any carry over to the rhesus blank sample. The results are summarized in supplemental Table 2.

Method validation: MA and its metabolites, as well as IS were separated from endogenous intervention peaks of the rhesus blank plasma matrix (Fig. 2A). The signal to noise ratio of extracted blank were found to be <5% of MA and its metabolites at the mean peak area ratio LLOQ and ULOQ with IS (Fig. 2A-D). The LLOQ for MA and its metabolites in plasma was obtained at 1.09 ng/mL. The mean LLOQ peak area ratios (analyte/IS) for MA, 4-OH MA, AM, 4-OH AM, and norephedrine were 0.0021, 0.0013, 0.0021, 0.0018, and 0.0015, respectively (Fig. 2B). Similarly the mean ULOQ peak area ratios for MA, 4-OH MA, AM, 4-OH AM and norephedrine were 1.1956, 1.8917, 1.7240, 0.7168, and 1.0796, respectively (Fig. 2C). An example of extracted validation QC sample of LQC, MQC, and HQC chromatogram peak area ratios of MA and its metabolites that were proportional to the

DMD Fast Forward. Published on October 9, 2014 as DOI: 10.1124/dmd.114.059378
This article has not been copyedited and formatted. The final version may differ from this version.

concentrations of two IS are shown in Fig. 2E-H. The LQC peak area ratios for MA, 4-OH MA, AM, 4-OH AM, and norephedrine were between 0.0226 and 0.0403 (Fig. 2E). Similarly, MQC and HQC peak area ratios for MA, 4-OH MA, AM, 4-OH AM and norephedrine ranged between 0.1167 and 0.3676, and 04391 and 1.4571, respectively (Fig. 2F and 2G). The extracted internal standard peak area is shown in Fig. 2H. Accuracy and precision were calculated using the best linear fit and least-square residuals for the standards. The assay was linear over the range of 1.09-800 ng/mL with R^2 (n=6) $\geq$ 0.9866. A regression equation and coefficient of determination were obtained as follows: MA: y = 0.0014x - 0.0011, 4-OH MA: y = 0.0017x + 0.0003, AM: y = 0.0018x - 0.0087, 4-OH AM: y = 0.0006x - 0.0075, and norephedrine: y = 0.001x + 0.0054. The accuracy and precision results of plasma were shown in Table 1 and for liver microsomes are shown in supplemental Table 3. The recovery, matrix effects, bench top, and freeze-thaw stabilities of these analytes in plasma and liver microsomes were measured. These results are shown in the Table 2, Table 3, supplemental Table 2 and supplemental Table 3.

MA metabolism in rhesus plasma: MA and its metabolites were determined at a linear range of 1.09-800 ng/mL levels in rhesus plasma. MA concentrations in two rhesus plasma samples were ~1-3 ng/mL. Surprisingly, the concentrations of both AM and 4-OH AM were ~30 ng/mL (Table 4). In contrast, the 4-OH MA concentration was <1 ng/mL and norephedrine was ≤3 ng/mL. The results demonstrated that AM and 4-OH AM are the major metabolites of MA. In addition, the relative concentrations of total MA metabolites were >40-fold higher than MA suggesting that MA metabolism is very rapid in rhesus macaque (Table 4).

MA metabolism in liver microsomes: The metabolism of MA in rhesus and human liver microsomes was examined by analyzing the levels of MA and its three metabolites, AM, 4OH AM, and 4-OH MA at different time points. Prior to measuring these analytes in

microsomes with LC-MS/MS method, we optimized the detection of these metabolites in liver microsomes by using SPE extraction. Upon optimization, these analytes also showed a sensitivity of 1.09 ng/mL for all metabolites in liver microsomes. MA metabolism for the N-demethylation and hydroxylation showed a pseudo-first order hyperbolic reaction (Fig. 3). Therefore, we determined maximum enzyme activity (highest product formation/substrate consumed) and apparent $t_{1/2}$ (time it takes for the formation of half the total products or consumption of half the total substrate) using equation for pseudo-first order hyperbolic reaction (Fig. 3A-D, Table 5). The maximum level of MA degradation in human microsomes was significantly lower than rhesus microsomes (40.1±11.1 vs. 60.0±5.1 ng/mL/mg microsomes) (Fig. 3B, Table 5). Furthermore, the apparent $t_{1/2}$ for MA in human was much higher than rhesus microsomes (7.18±4.7 vs. 1.46±0.41 hrs). Along with MA degradation, the maximum formation of AM in rhesus microsomes was significantly higher than human microsomes (35.5±4.2 vs. 27.5±3) (Fig. 3C and Table 5), however the formation of 4-OH AM was similar in both rhesus and human microsomes (Fig. 3D and Table 5). Furthermore, the $t_{1/2}$ of AM and 4-OH AM were significantly lower in human than rhesus microsomes (0.29±0.25 and 1.31±0.60 vs. 6.04±2.0 and 11.1±9.8, respectively) (Table 4). These results clearly suggest that the rate of MA metabolism is much higher in rhesus liver microsomes than the human microsomes. We further determined the kinetic parameters (V_{max} and K_m) for the formation of AM in human and monkey liver microsomes using both the (*l*- and *d*-) MA stereoisomers (Fig. 4). The K_m for *d*-MA was marginally different (no statistical significance) in human (15±4 µM) than in rhesus microsomes (27±11 µM). Similarly, the K_m for *l*-MA was also similar in both human (16±0.2 µM) and rhesus (16±4 µM). However, the V_{max} for both *d*-MA and *l*-MA in rhesus microsomes were ~6-fold higher (19 pM AM/min/mg microsomes for both stereoisomers) than human microsomes (3.5 and 3.1 pM AM/min/mg microsomes for *d*-MA and *l*-MA, respectively) (Fig 4). These results suggest that MA

DMD Fast Forward. Published on October 9, 2014 as DOI: 10.1124/dmd.114.059378
This article has not been copyedited and formatted. The final version may differ from this version.

metabolism in rhesus microsomes are catalytically more efficient (V_{max}/K_m) than in human microsomes.

Inhibition of MA metabolism by human CYP inhibitors: We determined the relative contributions of human CYP2D6 and CYP3A4 in MA metabolism for both the MA stereoisomers by using their specific inhibitors (quinidine, paroxetine and fluoxetine for CYP2D6 and ketoconazole, ritonavir and indinavir for CYP3A4) (Fig. 5). The results showed that human CYP2D6 inhibitors such as quinidine, paroxetine, and fluoxetine inhibited *d*-MA metabolism by approximately 35%, 27%, and 60%, respectively, while they inhibited *l*-MA metabolism by approximately 13%, 33%, and 20%., respectively. Similarly, human CYP3A4 inhibitors such as ketoconazole, ritonavir, and indinavir inhibited *d*-MA metabolism by approximately 50%, 30%, and 45%, respectively, while they inhibited *l*-MA metabolism by approximately 27%, 18%, and 22%, respectively. However, no significant inhibitions of either *d*- or *l*- MA metabolism was observed in rhesus microsomes by these human CYP2D6 and CYP3A4 inhibitors, except fluoxetine and indinavir for the metabolism of *d*-MA or *l*-MA, respectively (Fig. 5). These results clearly suggest that human CYP2D6 and CYP3A4 are different from their homologous enzymes (CYP2D6 and CYP3A64) in rhesus.

MA docking to human and rhesus CYP models: The differences observed in the inhibition of MA-metabolism using human versus rhesus microsomes may be due to different binding patterns of human and rhesus CYP3A4/3A64 and CYP2D6 enzymes. Therefore, we investigated the binding patterns of both *d*- and *l*-MA with human and rhesus CYP2D6 and CYP3A enzymes using substrate docking. The docking results showed that *d*-MA binds the active sites of all the four CYP enzymes in three different orientations (Table 6). From the top ten ranking in docking scores, the binding poses were classified into 3 cases: 1) the N-methyl group approaching to the heme iron, which would undergo N-demethylation, 2) the phenyl ring pointing to the heme iron, which would undergo hydroxylation at the C4 site, and

3) other atoms approaching to the heme iron, which would lead to other reactions. The detailed results have been summarized in Table 6. From the statistical data, human CYP2D6, rhesus CYP3A4, and rhesus CYP3A64 preferred both the cases (case 1 and 2), suggesting that these enzymes can yield both N-demethylation and 4-hydroxylation of MA. On the other hand, human CYP3A4 preferred only case 2, suggesting this enzyme can only yield N-demethylation. Further, based on the number of conformers, human CYP2D6 prefers 4-hydroxylation over N-demethylation, while rhesus CYP2D6 prefers N-demethylation over 4-hhydroxylation (Table 6, Fig. 6). However, both human and rhesus CYP3A4 mainly prefer N-demethylation. The results from docking energy and average distance from the heme to the site of reaction for all the CYP enzymes suggested that N-demethylation is preferred over 4-hydroxylation with both rhesus and human CYP2D6 and CYP3A enzymes. Furthermore, the results of *l*-MA docked into the active sites of four CYP enzymes were very similar to those of *d*-MA. The docking results of top ten binding poses for each CYP are summarized, as shown in supplemental data (Supplemental Table 7 and supplemental Fig. 1). Briefly, the binding poses of *l*-MA-docking were also classified into 3 cases, which are similar to those of *d*-MA. One point that is worth noting is that there was one binding pose leading to *l*-MA 4-hydroxylation by human CYP3A4, while no such binding pose was observed for *d*-MA. Similarly, there was no binding pose yielded for *l*-MA bond to rhesus CYP3A64, while one binding pose was observed for *d*-MA (supplemental data, Table 7 and Fig. 1).

DMD Fast Forward. Published on October 9, 2014 as DOI: 10.1124/dmd.114.059378
This article has not been copyedited and formatted. The final version may differ from this version.

DISCUSSION

In this study we developed and validated a reliable, rapid, simple, and sensitive ESI-tandem mass spectrometry method for simultaneous determination of MA and its four metabolites in rhesus plasma and liver microsomes. Surprisingly, the plasma levels of MA metabolites AM and 4-OHAM were much higher than MA and other metabolites. This finding was further confirmed in rhesus liver microsomes. In addition, we found that the metabolism of MA was more efficient in rhesus than human microsomes, suggesting differences in MA-metabolizing CYP enzymes between human and rhesus. The basis of these differences, in part, was supported by inhibition and docking studies. This is the first report on the metabolism of MA in rhesus and we demonstrate that the metabolism of MA is more rapid in rhesus than in humans.

LC-MS/MS is a widely used technique in clinical and preclinical research. However, LC-MS/MS results are often inconsistent because of ineffective optimization of MRM parameters, sample preparation, and extraction methods. These types of issues can be overcome by optimizing sample extraction and mass spectrometry parameters including MRM transitions with LC chromatogram conditions. Liquid-liquid and solid-phase extractions are usually the most effective approaches, however, they are expensive and time consuming (Earla et al., 2012). The elimination of water-soluble inorganic metallic substances, such as phosphates, sodium, and sulfates, from plasma are important in ESI LC-MS/MS analysis to reduce ion suppression (Bogusz et al., 2007; Clavijo et al., 2009). In addition, pH of the reconstitution solution and mobile phase are very important to achieve maximum chromatographic peak separation, resolution, reliability, ionization, and reproducibility. By considering all the above factors, we have validated a novel, rapid and robust ESI-LC-MS/MS assay by using hydrophilic-lipophilic balance SPE cartridge to analyze rhesus plasma. In this method we used 1 mL methanol followed by water which is

simpler and faster than the previously reported methods (Bogusz et al., 2007; Clavijo et al., 2009). In previously described methods, higher amount of solvents were used followed by additional washing steps that also contained NH_4OH, dichloromethane, and isopropanol. All previously reported LC-MS/MS methods have used ammonium acetate or ammonium formate buffers in their mobile phase systems with a proton adducts in negative and positive modes (Djozan and Baheri, 2007; Kim et al., 2008; Lee et al., 2012). Such ammoniated buffer mobile phase systems may enhance ionization of analytes. However, ammoniated buffers commonly clog the peak tubes, pump seals, and precipitate in the flow line of the mobile phase, which can lead to an increase in backup pressure causing leakage. Therefore, the optimization of MA and its metabolites in a formic acid mobile phase system, which does not clog the pump and maintains a uniform pressure, is superior to the previous method (Earla et al., 2012). Second, this mobile phase system is easy to clean because this mobile phase does not precipitate. Further, MA and its metabolites are all eluted and separated from the column within the same retention time (~1 min) with sharp resolution. Thus, this LC-MS/MS method is robust, fast, and effective compared with other published methods (Mueller et al., 2008), which has longer run time and asynchronous analyte elution. The *recovery efficiency* of this method is not only higher than the previous methods, but the peak response is reproducible and consistent. In addition, MA and its metabolites are very stable in freeze-thaw cycles at -80°C as well as in bench top at ambient temperature.

Using the newly developed LC-MS/MS technique, in rhesus plasma and liver microsomes we have shown that MA is rapidly metabolized to a major metabolite AM and a minor metabolite 4-OHAM in the liver microsomes. However, the levels of both the metabolites are similar, and >20-fold higher than MA in plasma when the rhesus macaque was treated for 20-weeks with MA. These results suggest that MA is first metabolized to AM through N-demethylation followed by conversion to 4-OH AM through 4-OH AM. In addition, our

results suggest that MA is also metabolized to 4-OH MA, which may be converted into 4-OH AM. Further, 4-OH AM metabolized into norephedrine. Thus in rhesus, which were treated for 20 weeks with MA, production of the major metabolite AM and the terminal metabolite 4-OH MA is expected, rather than only the production of AM as observed in liver microsomes treated for up to 12 hours by MA. This is the first *in vitro* as well as *in vivo* report on the MA metabolism in rhesus macaques. Our results are consistent with the literature, which report that MA is primarily metabolized to AM and 4-OH MA by N-demethylation and 4-hydroxylation, respectively in human and plasma and liver microsomes. AM is further metabolized to 4-OH AM and norephedrine by hydroxylation (Miranda et al., 2007; Mueller et al., 2008; de la Torre et al., 2012). Similarly, *in vitro* analysis of MA metabolism in human microsomes also suggest that MA is first metabolized to AM as the major metabolite and 4-OH AM as the minor metabolite. They also produce 4-OH MA, but its levels are too low to be able to determine its rate of formation (data not shown). As expected, norephedrine was not detectable in short reaction times in *in vitro* experiments using liver microsomes. However, norephedrine is expected to be formed in the plasma upon chronic treatment with MA as observed in rhesus plasma in the present study and in human as shown previously (Brodie et al., 1969; Lewander, 1971; Lin et al., 1997).

The most interesting observation in this study was the rate of MA metabolism, especially for the formation of AM, is much faster in rhesus liver microsomes than in human microsomes. Further, our kinetic study clearly suggests that rhesus microsomes are much more efficient (~8-fold when compared for V_{max}/K_m) than human microsomes for the formation of AM due to the metabolism of both *d*-MA and *l*-MA. However, there is no observable difference in the K_m between *d*-MA and *l*-MA suggesting that both the stereoisomers bind with similar affinity with either the human or rhesus enzymes. These differences could be as a result of differences in the CYP enzymes between human and rhesus. MA is mainly metabolized by

CYP2D6, and to some extent CYP3A4, in human liver (Ramamoorthy et al., 2001; de la Torre et al., 2012; Welter et al., 2013). However, our results from *in vitro* study using human microsomes show that CYP2D6 and CYP3A4 contribute almost equally to the metabolism of MA stereoisomers. Most importantly, human CYP2D6 and CYP3A4 inhibitors did not inhibit MA metabolism in rhesus microsomes. These results clearly suggest significant differences between human and rhesus MA-metabolizing CYP enzymes, which may also explain differences in catalytic properties of human and rhesus MA-metabolizing enzymes. Furthermore, it is possible that MA-metabolism in rhesus is attributed to entirely different CYP450 enzymes.

Species differences are expected to cause differences in drug metabolism between rhesus and humans (Kumar et al., 2009). Moreover, there is very little known about the rhesus homologues of human CYP2D6 and CYP3A4 (Selvakumar et al., 2014). Literature suggests that there is a rhesus homologue to human CYP2D6, which has >90% sequence homology (Yasukochi and Satta, 2011). However, the metabolic characteristics of rhesus macaque CYP2D6 have not been studied. Similarly, rhesus CYP3A64 is 93% identical to human CYP3A4 and also shows similar metabolic characteristics to human CYP3A4 for some substrates tested (Carr et al., 2006). In contrast, our results from MA metabolism, as well as inhibition by human CYP3A4 selective inhibitors, clearly suggest that rhesus CYP3A64 is different from the human CYP3A4. Similarly, the differences in MA metabolism and inhibition by human CYP2D6 selective inhibitors also suggest that rhesus CYP2D6 is different from human CYP2D6. Therefore, we developed rhesus CYP2D6 and CYP3A64 models using the crystal structures of human CYP2D6 and CYP3A64, respectively, and then docked these models with MA in the active site. The findings from docking studies are consistent with the experimental findings that AM is the major product and 4-OH MA or 4-OH AM are minor products in both human and rhesus microsomes. However, based on

docking data, it would be difficult to explain why rhesus CYP enzymes are more active than human CYP enzymes. To some extent, the docking data suggests that N-demethylation, which is the main reaction, is more preferred by rhesus CYP2D6 than the human CYP2D6. Similarly, the formation of 4-hydroxylation product is more preferred by rhesus CYP3A64 than human CYP3A4. Taken together, it can be suggested that CYP2D6 may be the major contributor of MA metabolism in rhesus, while in human both CYP2D6 and CYP3A4 may contribute equally.

In conclusion, we developed and validated a highly sensitive LC-MS/MS method for determining MA metabolism using rhesus plasma and liver microsomes, and the method was used for analysis of differential MA metabolism in rhesus and human. Overall our results suggest that rhesus MA metabolic CYP enzymes are different from human. Further studies are needed to understand structure-function relationships of rhesus CYP2D6 and CYP3A64 that contribute to rapid MA metabolism. It is also important to study whether CYP pathways-mediated MA metabolism contribute to oxidative stress and subsequent neurotoxicity in rhesus as well as in human.

DMD Fast Forward. Published on October 9, 2014 as DOI: 10.1124/dmd.114.059378
This article has not been copyedited and formatted. The final version may differ from this version.

ACKNOWLEDGMENTS

We appreciate Dr. Michael Kuhar for his support and input throughout the study.

AUTHORS CONTRIBUTION

Participated in research design: R. Earla, S. Kumar, H. Fox. W. Li, A. Kumar

Conducted experiments: R. Earla, L. Wang, S. Bosinger, J. Li, A. Shah, M. Gangwani, A. Nookala, X. Liu, L. Cao.

Contributed new reagents or analytic tools: R .Earla, W. Li.

Performed data analysis: R. Earla, S. Kumar, W. Li.

Wrote or contributed to the writing of the manuscript: R. Earla, S. Kumar, H. Fox, W. Li., A. Jackson, P. Silverstein, A. Kumar.

REFERENCES

Armstrong BD and Noguchi KK (2004) The neurotoxic effects of 3,4-methylenedioxymethamphetamine (MDMA) and methamphetamine on serotonin, dopamine, and GABA-ergic terminals: an in-vitro autoradiographic study in rats. *Neurotoxicology* **25:**905-914.

Berankova K, Habrdova V, Balikova M, and Strejc P (2005) Methamphetamine in hair and interpretation of forensic findings in a fatal case. *Forensic science international* **153:**93-97.

Bogusz MJ, Enazi EA, Hassan H, Abdel-Jawaad J, Ruwaily JA, and Tufail MA (2007) Simultaneous LC-MS-MS determination of cyclosporine A, tacrolimus, and sirolimus in whole blood as well as mycophenolic acid in plasma using common pretreatment procedure. *Journal of chromatography B, Analytical technologies in the biomedical and life sciences* **850:**471-480.

Brodie BB, Cho AK, Stefano FJ, and Gessa GL (1969) On mechanisms of norepinephrine release by amphetamine and tyramine and tolerance to their effects. *Advances in biochemical psychopharmacology* **1:**219-238.

Carr B, Norcross R, Fang Y, Lu P, Rodrigues AD, Shou M, Rushmore T, and Booth-Genthe C (2006) Characterization of the rhesus monkey CYP3A64 enzyme: species comparisons of CYP3A substrate specificity and kinetics using baculovirus-expressed recombinant enzymes. *Drug metabolism and disposition: the biological fate of chemicals* **34:**1703-1712.

Cherner M, Bousman C, Everall I, Barron D, Letendre S, Vaida F, Atkinson JH, Heaton R, Grant I, and Group H (2010) Cytochrome P450-2D6 extensive metabolizers are more vulnerable to methamphetamine-associated neurocognitive impairment: preliminary findings. *Journal of the International Neuropsychological Society : JINS* **16:**890-901.

Clavijo C, Strom T, Moll V, Betts R, Zhang YL, Christians U, and Bendrick-Peart J (2009) Development and validation of a semi-automated assay for the highly sensitive quantification of Biolimus A9 in human whole blood using high-performance liquid chromatography-tandem mass spectrometry. *Journal of chromatography B, Analytical technologies in the biomedical and life sciences* **877:**3506-3514.

de la Torre R, Yubero-Lahoz S, Pardo-Lozano R, and Farre M (2012) MDMA, methamphetamine, and CYP2D6 pharmacogenetics: what is clinically relevant? *Frontiers in genetics* **3:**235.

Djozan D and Baheri T (2007) Preparation and evaluation of solid-phase microextraction fibers based on monolithic molecularly imprinted polymers for selective extraction of diacetylmorphine and analogous compounds. *Journal of chromatography A* **1166:**16-23.

Dorman DC, Struve MF, Norris A, and Higgins AJ (2008) Metabolomic analyses of body fluids after subchronic manganese inhalation in rhesus monkeys. *Toxicological sciences : an official journal of the Society of Toxicology* **106:**46-54.

Earla R, Ande A, McArthur C, Kumar A, and Kumar S (2014) Enhanced nicotine metabolism in HIV-1-positive smokers compared with HIV-negative smokers: simultaneous determination of nicotine and its four metabolites in their plasma using a simple and sensitive electrospray ionization liquid chromatography-tandem mass spectrometry technique. *Drug metabolism and disposition: the biological fate of chemicals* **42:**282-293.

Earla R, Boddu SH, Cholkar K, Hariharan S, Jwala J, and Mitra AK (2010) Development and validation of a fast and sensitive bioanalytical method for the quantitative determination of glucocorticoids--quantitative measurement of dexamethasone in

rabbit ocular matrices by liquid chromatography tandem mass spectrometry. *Journal of pharmaceutical and biomedical analysis* **52:**525-533.

Earla R, Cholkar K, Gunda S, Earla RL, and Mitra AK (2012) Bioanalytical method validation of rapamycin in ocular matrix by QTRAP LC-MS/MS: application to rabbit anterior tissue distribution by topical administration of rapamycin nanomicellar formulation. *Journal of chromatography B, Analytical technologies in the biomedical and life sciences* **908:**76-86.

Edmund GH, Lewis DF, and Howlin BJ (2013) Modelling species selectivity in rat and human cytochrome P450 2D enzymes. *PloS one* **8:**e63335.

Fiser A and Sali A (2003) Modeller: generation and refinement of homology-based protein structure models. *Methods in enzymology* **374:**461-491.

Fitzgerald RL, Ramos JM, Jr., Bogema SC, and Poklis A (1988) Resolution of methamphetamine stereoisomers in urine drug testing: urinary excretion of R(-)-methamphetamine following use of nasal inhalers. *Journal of analytical toxicology* **12:**255-259.

Fitzmaurice PS, Tong J, Yazdanpanah M, Liu PP, Kalasinsky KS, and Kish SJ (2006) Levels of 4-hydroxynonenal and malondialdehyde are increased in brain of human chronic users of methamphetamine. *The Journal of pharmacology and experimental therapeutics* **319:**703-709.

Hendrickson H, Laurenzana E, and Owens SM (2006) Quantitative determination of total methamphetamine and active metabolites in rat tissue by liquid chromatography with tandem mass spectrometric detection. *The AAPS journal* **8:**E709-717.

Holder GE, McGary CM, Johnson EM, Zheng R, John VT, Sugimoto C, Kuroda MJ, and Kim WK (2014) Expression of the Mannose Receptor CD206 in HIV and SIV Encephalitis: A Phenotypic Switch of Brain Perivascular Macrophages with Virus Infection. *Journal of neuroimmune pharmacology : the official journal of the Society on NeuroImmune Pharmacology*.

Kim JY, Cheong JC, Ko BJ, Lee SK, Yoo HH, Jin C, and In MK (2008) Simultaneous determination of methamphetamine, 3,4-methylenedioxy-N-methylamphetamine, 3,4-methylenedioxy-N-ethylamphetamine, N,N-dimethylamphetamine, and their metabolites in urine by liquid chromatography-electrospray ionization-tandem mass spectrometry. *Archives of pharmacal research* **31:**1644-1651.

Koster RA, Alffenaar JW, Greijdanus B, VanDernagel JE, and Uges DR (2014) Fast and highly selective LC-MS/MS screening for THC and 16 other abused drugs and metabolites in human hair to monitor patients for drug abuse. *Therapeutic drug monitoring* **36:**234-243.

Kraemer T and Maurer HH (2002) Toxicokinetics of amphetamines: metabolism and toxicokinetic data of designer drugs, amphetamine, methamphetamine, and their N-alkyl derivatives. *Therapeutic drug monitoring* **24:**277-289.

Krasnova IN and Cadet JL (2009) Methamphetamine toxicity and messengers of death. *Brain research reviews* **60:**379-407.

Kumar A, Buch S, Foresman L, Bischofberger N, Lifson JD, and Narayan O (2001) Development of virus-specific immune responses in SHIV(KU)-infected macaques treated with PMPA. *Virology* **279:**97-108.

Kumar A, Lifson JD, Silverstein PS, Jia F, Sheffer D, Li Z, and Narayan O (2000) Evaluation of immune responses induced by HIV-1 gp120 in rhesus macaques: effect of vaccination on challenge with pathogenic strains of homologous and heterologous simian human immunodeficiency viruses. *Virology* **274:**149-164.

Kumar S, Qiu H, Oezguen N, Herlyn H, Halpert JR, and Wojnowski L (2009) Ligand diversity of human and chimpanzee CYP3A4: activation of human CYP3A4 by

lithocholic acid results from positive selection. *Drug metabolism and disposition: the biological fate of chemicals* **37:**1328-1333.

Larkin MA, Blackshields G, Brown NP, Chenna R, McGettigan PA, McWilliam H, Valentin F, Wallace IM, Wilm A, Lopez R, Thompson JD, Gibson TJ, and Higgins DG (2007) Clustal W and Clustal X version 2.0. *Bioinformatics* **23:**2947-2948.

Lee S, Kim J, In S, Choi H, Oh SM, Jang CG, and Chung KH (2012) Development of a simultaneous analytical method for selected anorectics, methamphetamine, MDMA, and their metabolites in hair using LC-MS/MS to prove anorectics abuse. *Analytical and bioanalytical chemistry* **403:**1385-1394.

Legrand N, Ploss A, Balling R, Becker PD, Borsotti C, Brezillon N, Debarry J, de Jong Y, Deng H, Di Santo JP, Eisenbarth S, Eynon E, Flavell RA, Guzman CA, Huntington ND, Kremsdorf D, Manns MP, Manz MG, Mention JJ, Ott M, Rathinam C, Rice CM, Rongvaux A, Stevens S, Spits H, Strick-Marchand H, Takizawa H, van Lent AU, Wang C, Weijer K, Willinger T, and Ziegler P (2009) Humanized mice for modeling human infectious disease: challenges, progress, and outlook. *Cell host & microbe* **6:**5-9.

Lewander T (1971) A mechanism for the development of tolerance to amphetamine in rats. *Psychopharmacologia* **21:**17-31.

Lin LY, Di Stefano EW, Schmitz DA, Hsu L, Ellis SW, Lennard MS, Tucker GT, and Cho AK (1997) Oxidation of methamphetamine and methylenedioxymethamphetamine by CYP2D6. *Drug metabolism and disposition: the biological fate of chemicals* **25:**1059-1064.

Melega WP, Jorgensen MJ, Lacan G, Way BM, Pham J, Morton G, Cho AK, and Fairbanks LA (2008) Long-term methamphetamine administration in the vervet monkey models aspects of a human exposure: brain neurotoxicity and behavioral profiles. *Neuropsychopharmacology : official publication of the American College of Neuropsychopharmacology* **33:**1441-1452.

Meyer MR, Peters FT, and Maurer HH (2008) The role of human hepatic cytochrome P450 isozymes in the metabolism of racemic 3,4-methylenedioxy-methamphetamine and its enantiomers. *Drug metabolism and disposition: the biological fate of chemicals* **36:**2345-2354.

Miranda GE, Sordo M, Salazar AM, Contreras C, Bautista L, Rojas Garcia AE, and Ostrosky-Wegman P (2007) Determination of amphetamine, methamphetamine, and hydroxyamphetamine derivatives in urine by gas chromatography-mass spectrometry and its relation to CYP2D6 phenotype of drug users. *Journal of analytical toxicology* **31:**31-36.

Moss JA, Malone AM, Smith TJ, Butkyavichene I, Cortez C, Gilman J, Kennedy S, Kopin E, Nguyen C, Sinha P, Hendry RM, Guenthner P, Holder A, Martin A, McNicholl J, Mitchell J, Pau CP, Srinivasan P, Smith JM, and Baum MM (2012) Safety and pharmacokinetics of intravaginal rings delivering tenofovir in pig-tailed macaques. *Antimicrobial agents and chemotherapy* **56:**5952-5960.

Moszczynska A and Yamamoto BK (2011) Methamphetamine oxidatively damages parkin and decreases the activity of 26S proteasome in vivo. *Journal of neurochemistry* **116:**1005-1017.

Mueller M, Peters FT, Ricaurte GA, and Maurer HH (2008) Liquid chromatographic-electrospray ionization mass spectrometric assay for simultaneous determination of 3,4-methylenedioxymethamphetamine and its metabolites 3,4-methylenedioxyamphetamine, 3,4-dihydroxymethamphetamine, and 4-hydroxy-3-methoxymethamphetamine in rat brain. *Journal of chromatography B, Analytical technologies in the biomedical and life sciences* **874:**119-124.

Nishimuta H, Sato K, Mizuki Y, Yabuki M, and Komuro S (2010) Prediction of the intestinal first-pass metabolism of CYP3A substrates in humans using cynomolgus monkeys. *Drug metabolism and disposition: the biological fate of chemicals* **38:**1967-1975.

Nishimuta H, Sato K, Mizuki Y, Yabuki M, and Komuro S (2011) Species differences in intestinal metabolic activities of cytochrome P450 isoforms between cynomolgus monkeys and humans. *Drug metabolism and pharmacokinetics* **26:**300-306.

Pendyala G, Trauger SA, Siuzdak G, and Fox HS (2011) Short communication: quantitative proteomic plasma profiling reveals activation of host defense to oxidative stress in chronic SIV and methamphetamine comorbidity. *AIDS research and human retroviruses* **27:**179-182.

Phillips KA, Bales KL, Capitanio JP, Conley A, Czoty PW, t Hart BA, Hopkins WD, Hu SL, Miller LA, Nader MA, Nathanielsz PW, Rogers J, Shively CA, and Voytko ML (2014) Why primate models matter. *American journal of primatology* **76:**801-827.

Ramamoorthy Y, Tyndale RF, and Sellers EM (2001) Cytochrome P450 2D6.1 and cytochrome P450 2D6.10 differ in catalytic activity for multiple substrates. *Pharmacogenetics* **11:**477-487.

Scanga CA and Flynn JL (2014) Modeling Tuberculosis in Nonhuman Primates. *Cold Spring Harbor perspectives in medicine*.

Selvakumar S, Bhutani P, Ghosh K, Krishnamurthy P, Kallipatti S, Selvam S, Ramarao M, Mandlekar S, Sinz MW, Rodrigues AD, and Subramanian M (2014) Expression and characterization of cynomolgus monkey cytochrome CYP3A4 in a novel human embryonic kidney cell-based mammalian system. *Drug metabolism and disposition: the biological fate of chemicals* **42:**369-376.

Sergi M, Bafile E, Compagnone D, Curini R, D'Ascenzo G, and Romolo FS (2009) Multiclass analysis of illicit drugs in plasma and oral fluids by LC-MS/MS. *Analytical and bioanalytical chemistry* **393:**709-718.

Shah A, Kumar S, Simon SD, Singh DP, and Kumar A (2013) HIV gp120- and methamphetamine-mediated oxidative stress induces astrocyte apoptosis via cytochrome P450 2E1. *Cell death & disease* **4:**e850.

Thompson PM, Hayashi KM, Simon SL, Geaga JA, Hong MS, Sui Y, Lee JY, Toga AW, Ling W, and London ED (2004) Structural abnormalities in the brains of human subjects who use methamphetamine. *The Journal of neuroscience : the official journal of the Society for Neuroscience* **24:**6028-6036.

Thurman EM, Pedersen MJ, Stout RL, and Martin T (1992) Distinguishing sympathomimetic amines from amphetamine and methamphetamine in urine by gas chromatography/mass spectrometry. *Journal of analytical toxicology* **16:**19-27.

Uno Y, Matsushita A, Shukuya M, Matsumoto Y, Murayama N, and Yamazaki H (2014) CYP2C19 polymorphisms account for inter-individual variability of drug metabolism in cynomolgus macaques. *Biochemical pharmacology* **91:**242-248.

Uno Y, Uehara S, Kohara S, Murayama N, and Yamazaki H (2010) Cynomolgus monkey CYP2D44 newly identified in liver, metabolizes bufuralol, and dextromethorphan. *Drug metabolism and disposition: the biological fate of chemicals* **38:**1486-1492.

Welter J, Meyer MR, Wolf EU, Weinmann W, Kavanagh P, and Maurer HH (2013) 2-methiopropamine, a thiophene analogue of methamphetamine: studies on its metabolism and detectability in the rat and human using GC-MS and LC-(HR)-MS techniques. *Analytical and bioanalytical chemistry* **405:**3125-3135.

Wongniramaikul W, Choodum A, Dennany L, and Nic Daeid N (2012) A comprehensive chromatographic comparison of amphetamine and methylamphetamine extracted from river water using molecular imprinted polymers and without the need for sample derivatization. *Journal of separation science* **35:**3332-3339.

Yasukochi Y and Satta Y (2011) Evolution of the CYP2D gene cluster in humans and four non-human primates. *Genes & genetic systems* **86:**109-116.

DMD Fast Forward. Published on October 9, 2014 as DOI: 10.1124/dmd.114.059378
This article has not been copyedited and formatted. The final version may differ from this version.

FOOTNOTES

The work was funded by the National Institute on Drug Abuse [DA025528] and [DA025011] to A. Kumar and National Natural Science Foundation of China [81373328] to W. Li.

DMD Fast Forward. Published on October 9, 2014 as DOI: 10.1124/dmd.114.059378
This article has not been copyedited and formatted. The final version may differ from this version.

FIGURE LEGENDS

Figure 1: Development of LC-MS/MS method to quantitate methamphetamine (MA) and four of its metabolites in rhesus plasma. MS/MS spectra of **A.** MA, **B.** 4-hydroxymethamphetamine (4-OH MA), **C.** amphetamine (AM), **D.** 4-hydroxyamphetamine (4-OH AM), and **E.** norephedrine, **F.** methamphetamine-d5(IS) and **G**. amphetamine-d8 (IS) with ESI proton adducts $[M+H]^+$ in positive mode, and **H**. Simultaneous analysis of multiple reaction monitoring (MRM) chromatogram peaks of a mixture of reference standard containing MA, 4-OH MA, AM, 4-OH AM, norephedrine, MA-d5(IS) and AM-d8 (IS) which were separated based on their *mass* to *charge(m/z).* Y-axis shows intensity (CPS, count per second); X-axis shows *mass* to *charge* ratio (*m/z*, amu) in **A-G** and run time (min) in **H**.

Figure 2: Concurrent analysis of LC-MS/MS-MRM chromatogram peaks of methamphetamine (MA), 4-hydroxymethamphetamine (4-OH MA), amphetamine (AM), 4-hydroxyamphetamine (4-OH AM), and norephedrine, MA-d5 (IS) and AM-d8 (IS) in rhesus plasma: **A**. extracted blanks; **B**. extracted lower limit of quantitation (LLOQ, 1.09 ng/mL); **C**. Extracted upper limit of quantification (ULOQ, 800 ng/mL); **D**. Extracted deuterated internal standards; **E**. Extracted low quality control (LQC, 14.94 ng/mL) standard; **F**. Extracted middle quality control (MQC, 214.0 ng/mL); **G.** Extracted high quality control (HQC, 800 ng/mL), and **H**. Extracted deuterated internal standards. PAR: peak area ratio (analyte/IS); PA: peak area; IS: internal standard; Y-axis shows intensity (CPS, count per second); X-axis shows run time (min).

Figure 3: Kinetics of methamphetamine (MA) degradation and formation of its metabolites, amphetamine (AM) and 4-hydroxyamphetamine (4-OH AM) in rhesus liver microsomes and human liver microsomes. **A**. MA remaining amount (ng/mL); **B**. MA degradation (ng/mL);

C. Formation AM, and D. Formation of 4-OH MA. The degradation of MA was plotted by using the remaining amount of MA **(A)** and by using the amount that was metabolized **(B)**. The enzyme activities were performed using human and rhesus microsomes as described in Materials and Methods. The maximum activity and apparent $t_{1/2}$ were determined by fitting the data using hyperbolic equation. LM: liver microsomes.

Figure 4: Substrate kinetic studies using both enantiomers of methamphetamine (*d*- and *l*-MA) and determination of kinetic parameters K_m and V_{max} of human and monkey microsomes) for formation of AM. The velocity of formation of amphetamine (pM AM/min/mg liver microsomes (LM)) are shown on Y-axis and MA concentrations (μM) on X-axis. **A**. Formation of AM in human and monkey liver microsomes with *d*-MA; **B.** Formation of AM in human and monkey liver microsomes with *l*-MA. The kinetic parameters K_m and V_{max} were determined by fitting the curve to non-linear regression analysis using Michaelis-Menten model, and the data are presented in the inset. Mean **±** SEM were calculated from the fitting of the curve.

Figure 5: Enzyme inhibition using selective inhibitors of human CYP2D6 (quinidine (QND), paroxetine (PXN), and fluoxetine (FXN) and CYP3A4 (ketoconazole (KTZ), ritonavir (RTV), and indinavir (INV). The formation of amphetamine (AM) was determined in the absence and presence of these inhibitors in rhesus and human liver microsomes. **A**. Formation of AM in human liver microsomes at 1 hr; **B**. Formation of AM in rhesus liver microsomes at 1 hr. Y-axis represent the percentage of AM formation (mean + S.E). The 100% activity in human and rhesus corresponds to ~ 2ng/mL/mg LM and ~11 ng/mL/mg LM, respectively.

DMD Fast Forward. Published on October 9, 2014 as DOI: 10.1124/dmd.114.059378
This article has not been copyedited and formatted. The final version may differ from this version.

Figure 6. Autodocking of MA with human CY3A4, rhesus CYP3A64, human CYP2D6, and rhesus CYP2D6. The figures shows the: 1) binding of methamphetamine (MA) with human CYP2D6 active site in orientation leading N-demethylation (**A**) and 4-hydroxylation (B), 2) binding of MA with rhesus CYP2D6 in orientation leading to N-demethylation (**C**) and 4-hydroxylation (**D**), 3) binding of human CYP3A4 in orientation leading to N-demethylation in two different binding modes (**E-F**) and 4-hydroxylation (**G-H**). Human CYP3A4 and rhesus CYP3A64 both binds to MA in the same orientation (N-demethylation), but in two different binding modes. Structure of MA is shown in blue, amino acid residues of CYP enzymes are shown in green, and heme of the enzyme is shown in red.

Table 1. Between day precision and accuracy of calibration curve standards (CC, n=6) and four level quality control (QC, n=18) standards for methamphetamine, 4-hydroxymethamphetamine, amphetamine, 4-ydroxyamphetamine and norephedrine in monkey plasma.

Name	Nominal conc.	CC-1	CC-2	CC-3	CC-4	CC-5	CC-6	CC-7	CC-8	CC-9	HQC	MQC	LQC	LLOQ
	(ng/mL)	800	640	486.4	389.1	214	74.9	14.9	4.94	1.09	640	214	14.9	1.09
MA	Actual (ng/mL)	827.8	655.4	447.4	383.5	228.3	84.1	15.6	5.35	1.2	544.6	205.9	15.2	1
	% Accuracy	103.5	102.4	92	98.6	106.4	112.2	104.7	108.3	110.1	85.1	96.2	101.5	91.9
	% CV	7.8	10.1	11.7	14.8	4.3	18.1	9.6	9	9.6	13.7	11.5	7.6	23.1
4-OH MA	Actual (ng/mL)	869.7	605.4	497.4	383.3	228.2	83.9	15.5	5.34	1.23	578	214.4	15.3	1.1
	% Accuracy	108.7	94.6	102.3	98.7	106.7	112.3	104.5	108.3	112.8	90.3	100.2	102.1	100.9
	% CV	10.8	16.3	17.5	14.6	4.3	17.9	9.5	9.1	12.2	14.06	10.91	6.78	21.2
AM	Actual (ng/mL)	807.8	655.7	445.3	385.8	240.8	75.5	15.2	4.5	1.28	549.2	212.6	14.6	0.97
	% Accuracy	101	102.5	91.6	99.2	112.5	100.8	102	91.1	117.4	85.8	99.3	97.5	89.4
	% CV	7.1	8.7	10.2	12.8	8.1	10.4	10.6	19	8.6	13.5	10.4	10.4	27.2
4-OH AM	Actual (ng/mL)	779.4	671.7	465.3	439.8	245	78.7	16	4.7	1.29	560.6	232.7	15.4	1.06
	% Accuracy	97.4	105	95.7	113	114.5	105.1	106.7	95.2	118.5	87.6	108.7	102.8	97.6
	% CV	9	10.8	13	7.8	18.6	14.6	8.9	20.5	1.4	12.5	15.7	9.6	17
Norephedrine	Actual (ng/mL)	787.8	635.7	425.3	399.8	244.8	74.7	15.6	4.7	1.29	584.6	210.3	15.6	1.06
	% Accuracy	98.5	99.3	87.4	102.7	114.4	99.7	104	95.2	118.5	91.3	98.3	104.1	97.6
	% CV	7.6	9.2	11.2	7.2	7.6	9.4	12.7	16.2	6.6	15.4	10.2	6.2	19.5

MA=methamphetamine; 4-OH MA=4-hydroxymethamphetamine; AM=Amphetamine; 4-OH AM=4-hydroxyamphetamine; LLOQ=lower limit of quantitation; LQC=lower QC; MQC=Middle QC; HQC=High QC; CV (Precision) = coefficient of variation; All CC and QC standard concentration values were presented in one decimal place except CC-8 and 9, and LQC and LLOQ which were presented in two decimal places.

Table 2. Recovery and matrix effect of two levels of quality control (QC, n=6) standards for MA, 4-OH MA, AM, 4-OH AM and norephedrine in monkey plasma.

		Recovery		Matrix effect	
Name	Name conc.	HQC	LQC	HQC	LQC
	(ng/mL)	640.0	14.94	640.0	14.94
MA	Actual (ng/mL)	827.8	655.4	447.4	383.5
	% Accuracy	103.5	102.4	92.0	98.6
	% CV	7.8	10.1	11.7	14.8
4-OH MA	Actual (ng/mL)	869.7	605.4	497.4	383.3
	% Accuracy	108.7	94.6	102.3	98.7
	% CV	10.8	16.3	17.5	14.6
AM	Actual (ng/mL)	807.8	655.7	445.3	385.8
	% Accuracy	101.0	102.5	91.6	99.2
	% CV	7.1	8.7	10.2	12.8
4-OH AM	Actual (ng/mL)	779.4	671.7	465.3	439.8
	% Accuracy	97.4	105.0	95.7	113.0
	% CV	9.0	10.8	13.0	7.8
Norephedrine	Actual (ng/mL)	787.8	635.7	425.3	399.8
	% Accuracy	98.5	99.3	87.4	102.7
	% CV	7.6	9.2	11.2	7.2

MA=methamphetamine; 4-OH MA=4-hydroxymethamphetamine; AM=Amphetamine; 4-OH AM=4-hydroxyamphetamine; LLOQ=lower limit of quantitation; LQC=lower QC; MQC=Middle QC; HQC=High QC; CV (Precision)= coefficient of variation; All CC and QC standard values were presented in one decimal place except CC-8 and 9, and LQC and LLOQ which were presented in two decimal places.

Table 3. Bench top (25^0C) and Freeze thaw (-80^0C) for stability four cycle quality control (QC, n=6) standards of methamphetamine; 4-hydroxymethamphetamine; Amphetamine; 4-hydroxyamphetamine and norephedrine in plasma.

		Bench top (25^0C)		Freeze thaw (-80^0C)	
Name	Name conc.	HQC	LQC	HQC	LQC
	(ng/mL)	640.0	14.94	640.0	14.94
MA	Actual (ng/mL)	827.8	655.4	447.4	383.5
	% Accuracy	103.5	102.4	92.0	98.6
	% CV	7.8	10.1	11.7	14.8
4-OH MA	Actual (ng/mL)	869.7	605.4	497.4	383.3
	% Accuracy	108.7	94.6	102.3	98.7
	% CV	10.8	16.3	17.5	14.6
AM	Actual (ng/mL)	807.8	655.7	445.3	385.8
	% Accuracy	101.0	102.5	91.6	99.2
	% CV	7.1	8.7	10.2	12.8
4-OH AM	Actual (ng/mL)	779.4	671.7	465.3	439.8
	% Accuracy	97.4	105.0	95.7	113.0
	% CV	9.0	10.8	13.0	7.8
Norephedrine	Actual (ng/mL)	787.8	635.7	425.3	399.8
	% Accuracy	98.5	99.3	87.4	102.7
	% CV	7.6	9.2	11.2	7.2

MA=methamphetamine; 4-OH MA=4-hydroxymethamphetamine; AM=Amphetamine; 4-OH AM=4-hydroxyamphetamine; LLOQ=lower limit of quantitation; LQC=lower QC; MQC=Middle QC; HQC=High QC; CV (Precision)= coefficient of variation; All CC and QC standard values were presented in one decimal place except CC-8 and 9, and LQC and LLOQ which were presented in two decimal places.

Table 4. Determination of the methamphetamine and its metabolites 4-hydroxymethamphetamine, amphetamine, 4-hydroxyamphetamine and norephedrine in the rhesus monkey plasma after administration of methamphetamine for 20 weeks.

Drug/metabolites	Monkey-1 (ng/mL)	Monkey-2 (ng/mL)
Methamphetamine	2.83	1.22
4-Hydroxymethamphetamine	0.28	0.24
Amphetamine	29.7	28.4
4-Hydroxyamphetamine	27.3	30.1
Norephedrine	2.11	2.39

Table 5. Determination of apparent kinetic constants of the microsomal N-demethylation and hydroxylation of methamphetamine into amphetamine and 4-hydroxyamphetamine in rhesus monkey and human.

	Monkey microsomes		Human microsomes		Ratio: Monkey/Human
Name	Activity (ng/mL/mg HM)	Apparent ($t_{1/2}$), Hrs)	Activity (ng/mL/mg HM)	Apparent ($t_{1/2}$, Hrs)	Relative activity/($t_{1/2}$)
MA	67.9±5.1	1.46±0.41	40.1±11	7.18±4.7	8.34
AM	35.5±4.2	0.29±0.25	27.3±4.5	6.04±2.0	27.1
4-OH AM	4.79±0.61	1.31±0.60	4.57±1.9	11.1±9.8	9.00

Apparent kinetic constants for the hydroxylation and N-demethylation of methamphetamine by hepatic microsomes (HM) from human and monkey were obtained by measuring the consumption of methamphetamine and formation of metabolites.

Table 6. The statistical results of MA docked into the active sites of four CYP enzymes

CYPs	SOM1 (4-OH)				SOM2 (de-methyl)				Other
	No of conf	Average score [a]	Lowest score	Average distance (Å) [b]	No of conf	Average score	Lowest score	Average distance (Å)[b]	No of conf
Human CYP2D6	6	-5.65	-5.87	3.54	2	-5.447	-5.485	3.16	2
Rhesus CYP2D6	3	-5.1	-5.38	3.86	4	-4.95	-5.04	3.31	3
Human CYP3A4	0	0	0	0	8	-5.12	-5.62	3.42	2
Rhesus CYP3A64	1	-5.58	-5.58	3.43	7	-5.39	-5.87	3.27	2

[a] The average docking scores of all poses in this case.

[b] The average distance between C4 in the phenyl ring or the C atom of the N-methyl group.

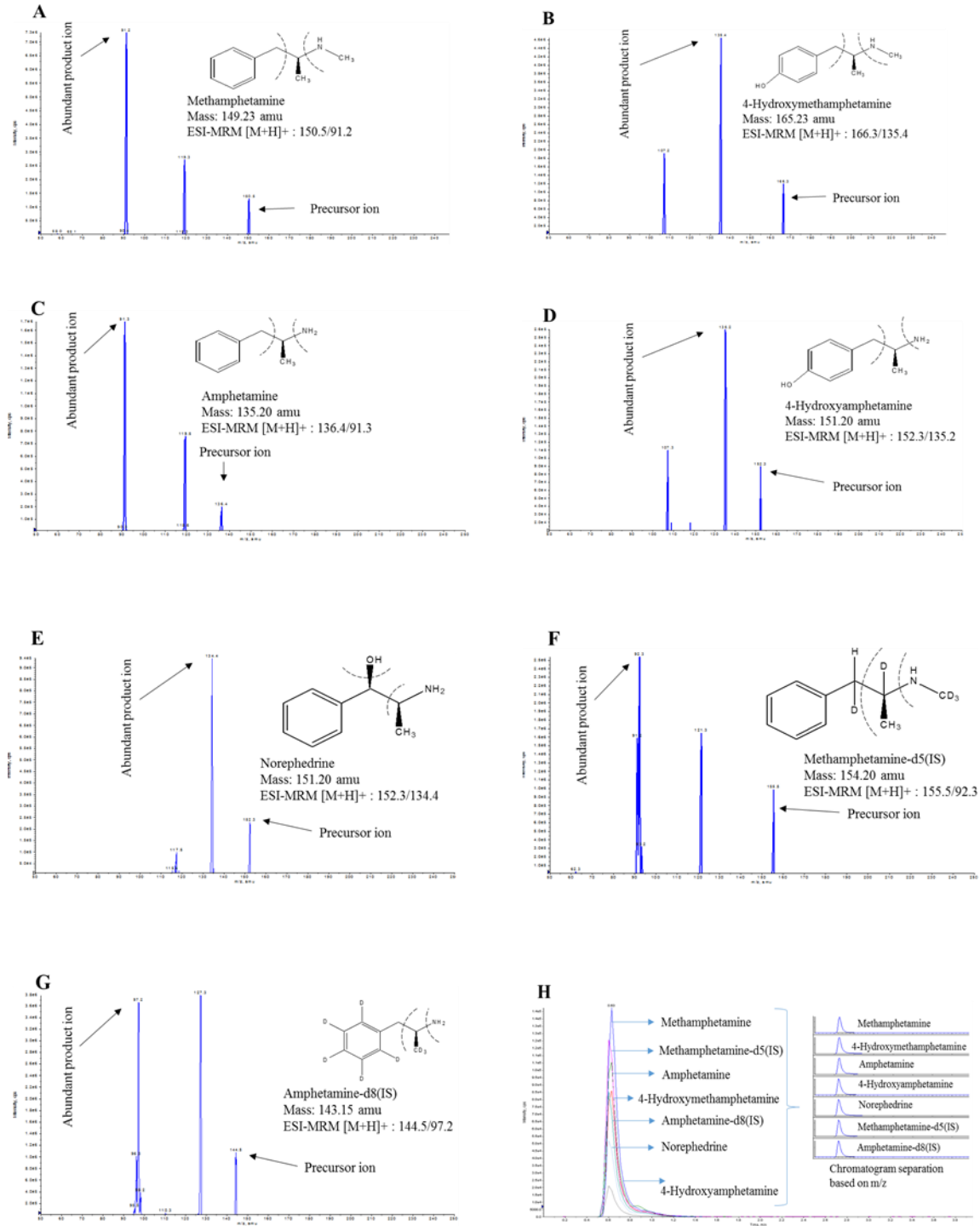
A
Abundant product ion
Methamphetamine
Mass: 149.23 amu
ESI-MRM [M+H]+ : 150.5/91.2
Precursor ion
B
Abundant product ion
4-Hydroxymethamphetamine
Mass: 165.23 amu
ESI-MRM [M+H]+ : 166.3/135.4
Precursor ion
C
Abundant product ion
Amphetamine
Mass: 135.20 amu
ESI-MRM [M+H]+ : 136.4/91.3
Precursor ion
D
Abundant product ion
4-Hydroxyamphetamine
Mass: 151.20 amu
ESI-MRM [M+H]+ : 152.3/135.2
Precursor ion
E
Abundant product ion
Norephedrine
Mass: 151.20 amu
ESI-MRM [M+H]+ : 152.3/134.4
Precursor ion
F
Abundant product ion
Methamphetamine-d5(IS)
Mass: 154.20 amu
ESI-MRM [M+H]+ : 155.5/92.3
Precursor ion
G
Abundant product ion
Amphetamine-d8(IS)
Mass: 143.15 amu
ESI-MRM [M+H]+ : 144.5/97.2
Precursor ion
H
Methamphetamine
Methamphetamine-d5(IS)
Amphetamine
4-Hydroxymethamphetamine
Amphetamine-d8(IS)
Norephedrine
4-Hydroxyamphetamine
Chromatogram separation based on m/z

Figure 1


A
Blank : Methamphetamine
Q1/Q3: m/z[150.5/91.2]
Blank: 4-Hydroxymethamphetamine
Q1/Q3: m/z[166.3/135.4]
Blank: Amphetamine
Q1/Q3: m/z[136.4/91.3]
Blank: 4-Hydroxyamphetamine
Q1/Q3: m/z[152.3/135.2]
Blank : Norephedrine
Q1/Q3: m/z[152.3/134.4]
B
Methamphetamine
Q1/Q3: m/z[150.5/91.2]
LLOQ: 1.09ng/mL; PAR: 0.0021
4-Hydroxymethamphetamine
Q1/Q3: m/z[166.3/135.4]
LLOQ: 1.09ng/mL; PAR: 0.0013
Amphetamine
Q1/Q3: m/z[136.4/91.3]
LLOQ: 1.09ng/mL; PAR: 0.0021
4-Hydroxyamphetamine
Q1/Q3: m/z[152.3/135.2]
LLOQ: 1.09ng/mL; PAR: 0.0018
Norephedrine
Q1/Q3: m/z[152.3/134.4]
LLOQ: 1.09ng/mL; PAR: 0.0015
C
Methamphetamine
Q1/Q3: m/z[150.5/91.2]
ULOQ: 800ng/mL; PAR: 1.1956
4-Hydroxymethamphetamine
Q1/Q3: m/z[166.3/135.4]
ULOQ: 800ng/mL; PAR: 1.1817
Amphetamine
Q1/Q3: m/z[136.4/91.3]
ULOQ: 800ng/mL; PAR:1.7240
4-Hydroxyamphetamine
Q1/Q3: m/z[152.3/135.2]
ULOQ: 800ng/mL; PAR: 0.7168
Norephedrine
Q1/Q3: m/z[152.3/134.4]
ULOQ: 800ng/mL; PAR: 1.0796
D
Methamphetamine-d5
Q1/Q3: m/z[155.5/92.3]
IS: 1µg/mL; PA: 248990
Methamphetamine-d5
Q1/Q3: m/z[155.5/92.3]
IS: 1µg/mL; PA: 248990
Amphetamine-d8
Q1/Q3: m/z[144.5/97.2]
IS: 1µg/mL; PA: 240644
Amphetamine-d8
Q1/Q3: m/z[144.5/97.2]
IS: 1µg/mL; PA: 240644
Amphetamine-d8
Q1/Q3: m/z[144.5/97.2]
IS: 1µg/mL; PA: 240644
E
Methamphetamine
Q1/Q3: m/z[150.5/91.2]
LQC: 14.98ng/mL; PAR: 0.0226
4-Hydroxymethamphetamine
Q1/Q3: m/z[166.3/135.4]
LQC: 14.98ng/mL; PAR: 0.0296
Amphetamine
Q1/Q3: m/z[136.4/91.3]
LQC: 14.98ng/mL; PAR: 0.0403
4-Hydroxyamphetamine
Q1/Q3: m/z[152.3/135.2]
LQC: 14.98ng/mL; PAR: 0.0105
Norephedrine
Q1/Q3: m/z[152.3/134.4]
LQC: 14.98ng/mL; PAR: 0.0178
F
Methamphetamine
Q1/Q3: m/z[150.5/91.2]
MQC: 214.02ng/mL; PAR: 0.2582
4-Hydroxymethamphetamine
Q1/Q3: m/z[166.3/135.4]
MQC: 214.02ng/mL; PAR: 0.2631
Amphetamine
Q1/Q3: m/z[136.4/91.3]
MQC: 214.02ng/mL; PAR: 0.3676
4-Hydroxyamphetamine
Q1/Q3: m/z[152.3/135.2]
MQC: 214.02ng/mL; PAR: 0.1167
Norephedrine
Q1/Q3: m/z[152.3/134.4]
MQC: 214.02ng/mL; PAR: 0.2316
G
Methamphetamine
Q1/Q3: m/z[150.5/91.2]
HQC: 640.00ng/mL; PAR: 1.0052
4-Hydroxymethamphetamine
Q1/Q3: m/z[166.3/135.4]
HQC: 640.00ng/mL; PAR: 1.0140
Amphetamine
Q1/Q3: m/z[136.4/91.3]
HQC: 640.00ng/mL; PAR: 1.4571
4-Hydroxyamphetamine
Q1/Q3: m/z[152.3/135.2]
HQC: 640.00ng/mL; PAR:
0.4391
Norephedrine
Q1/Q3: m/z[152.3/134.4]
HQC: 640.00ng/mL; PAR: 0.8861
H
Methamphetamine-d5
Q1/Q3: m/z[155.5/92.3]
IS: 1µg/mL; PA: 210389
Methamphetamine-d5
Q1/Q3: m/z[155.5/92.3]
IS: 1µg/mL; PA: 210349
Amphetamine-d8
Q1/Q3: m/z[144.5/97.2]
IS: 1µg/mL; PA: 209541
Amphetamine-d8
Q1/Q3: m/z[144.5/97.2]
IS: 1µg/mL; PA: 209541
Amphetamine-d8
Q1/Q3: m/z[144.5/97.2]
IS: 1µg/mL; PA: 209541

Figure 2

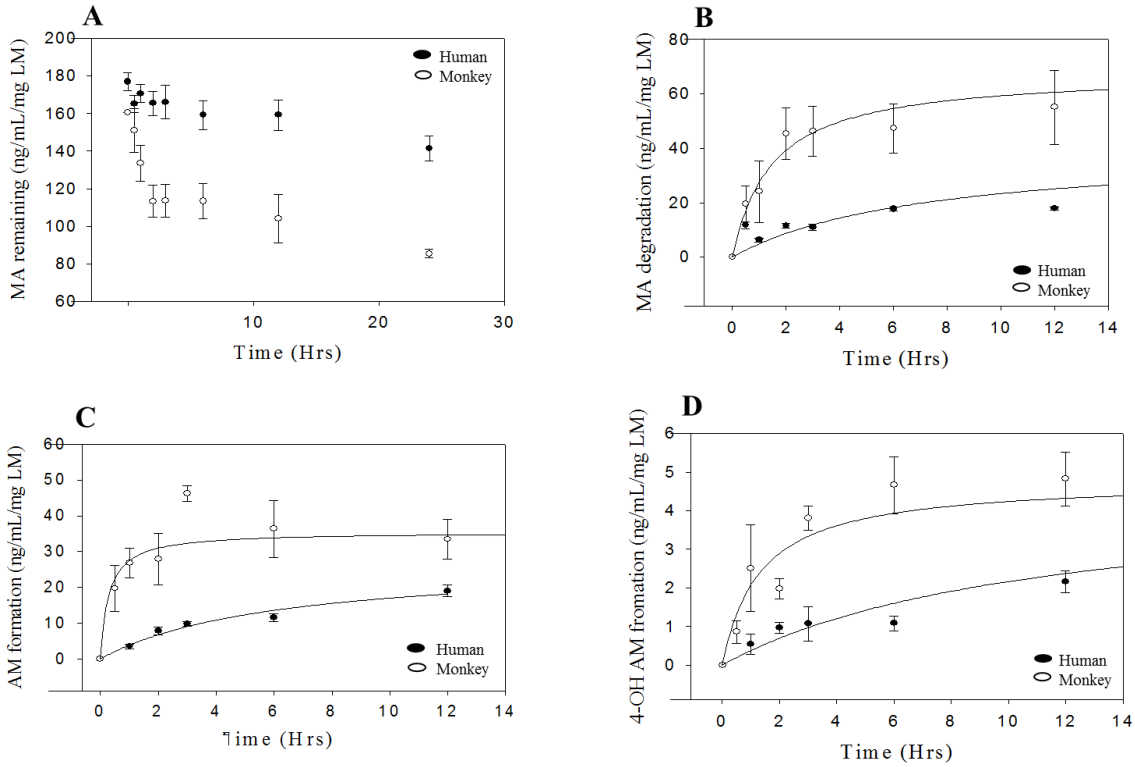
A
MA remaining (ng/mL/mg LM)
Time (Hrs)
Human
Monkey
B
MA degradation (ng/mL/mg LM)
Time (Hrs)
Human
Monkey
C
AM formation (ng/mL/mg LM)
Time (Hrs)
Human
Monkey
D
4-OH AM fromation (ng/mL/mg LM)
Time (Hrs)
Human
Monkey

Figure 3

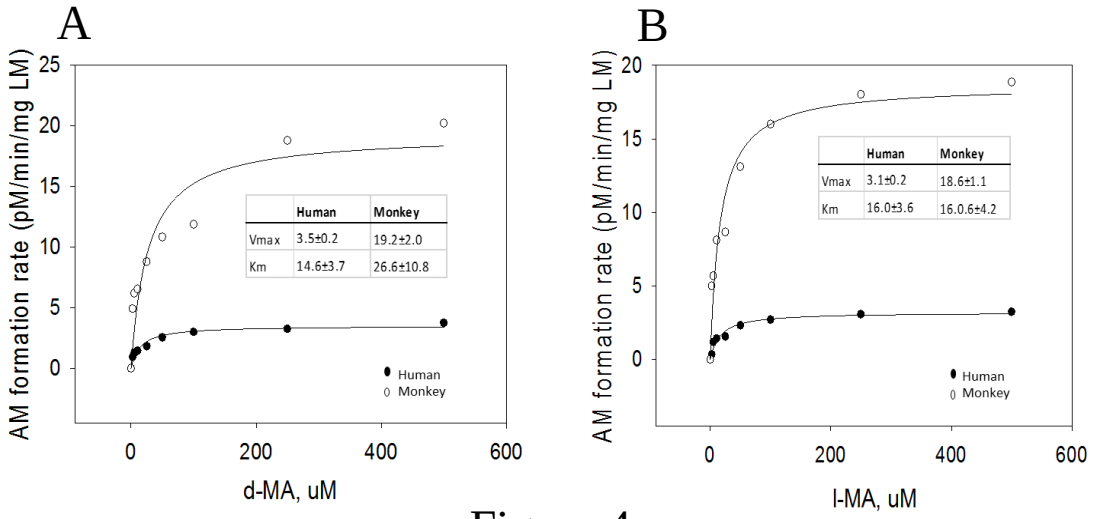
A
AM formation rate (pM/min/mg LM)
25
20
15
10
5
0
0
200
400
600
d-MA, uM
Human
Monkey
Vmax
Km
3.5±0.2
19.2±2.0
14.6±3.7
26.6±10.8
B
AM formation rate (pM/min/mg LM)
20
15
10
5
0
0
200
400
600
l-MA, uM
Human
Monkey
Vmax
Km
3.1±0.2
18.6±1.1
16.0±3.6
16.0.6±4.2

Figure 4

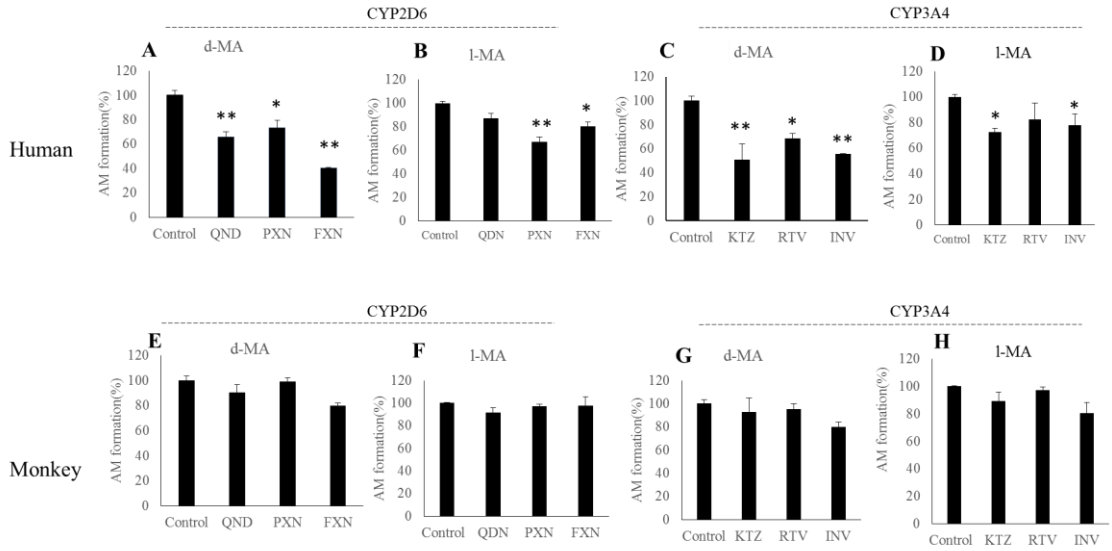
Human
Monkey
CYP2D6
CYP3A4
A
d-MA
B
l-MA
C
d-MA
D
l-MA
E
d-MA
F
l-MA
G
d-MA
H
l-MA
AM formation(%)
Control
QND
QDN
PXN
FXN
KTZ
RTV
INV

Figure 5

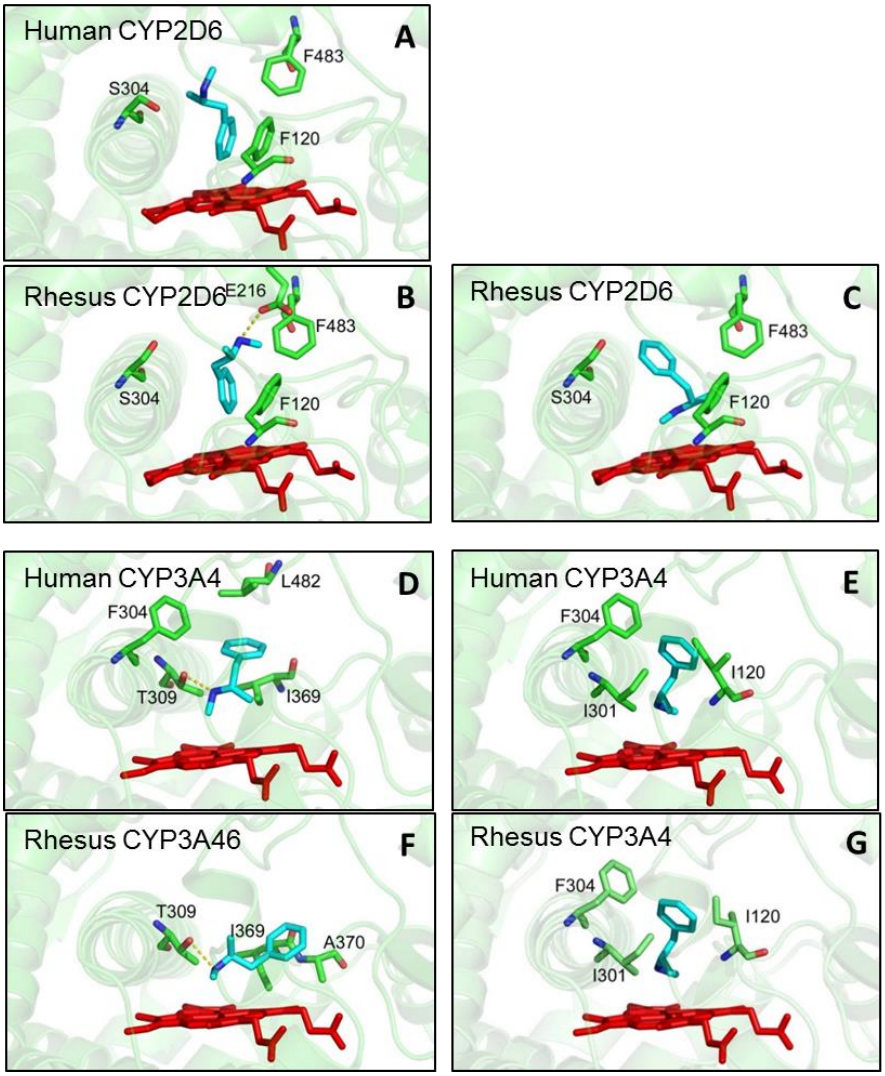
Human CYP2D6
A
F483
S304
F120
Rhesus CYP2D6 E216
B
F483
S304
F120
Rhesus CYP2D6
C
F483
S304
F120
Human CYP3A4
L482
D
F304
T309
I369
Human CYP3A4
E
F304
I120
I301
Rhesus CYP3A46
F
T309
I369
A370
Rhesus CYP3A4
G
F304
I120
I301

Figure 6